NUMERICAL SIMULATION OF PRESSURE DISTRIBUTION AROUND A HETEROGENEOUS NUCLEATION SITE

Lilac Cuiling Wang, Siu N. Leung, Chul B. Park and Markus Bussmann
Department of Mechanical & Industrial Engineering, University of Toronto
Toronto, Ontario, Canada M5S 3G8

Abstract

Pressure is a critical parameter that affects the degree of supersaturation within a polymer-gas solution when foaming. In most previous studies on cell nucleation, a uniform pressure throughout the solution was assumed. Although this assumption may be acceptable when no nucleating agent has been added, its validity is questionable when nucleating agents are present. The discontinuity at the interface between the nucleating agent and surrounding material is a potential heterogeneous nucleation site, and so the stress field around a particle will be different from the bulk. In light of this, this paper presents a numerical analysis to investigate the pressure profile around cell nucleating agents. Such an investigation is expected to provide new insights to understand cell nucleation phenomena.

Introduction

Nucleating agents have long been employed in polymeric foaming processes to promote cell nucleation in order to increase cell density, reduce cell size, and improve cell uniformity. Such desirable cell morphology will translate into notable advantages in various applications, ranging from household products to advanced engineering applications. Comparing plastic foams to their solid counterparts, they can be customized to offer improved mechanical [1-2], thermal [3], acoustical [4], and optical properties [5]. Furthermore, the addition of nucleating agents can help to reduce the material usage, which typically accounts for 70% of the production cost of foam products.

Using the classical thermodynamics, it has been proven that the presence of heterogeneous nucleating sites of various shapes will help to reduce the free energy barrier to initiate cell nucleation [6-9], and thereby aid in generating more cells. This was the basis of various theoretical studies [10-16] of polymeric foaming processes over the past few decades. In these studies, researchers used the system pressure in the foaming equipment to approximate the pressure inside the polymer-gas solution during foaming processes, but this assumption ignored the local pressure fluctuation. Instead, it is believed that during a polymeric foaming process, either the local movement of the polymer-gas solution caused by the expansion of a nucleated bubble, or the flow of the polymer-gas solution in an extrusion die will induce a stress field within the polymer matrix. The discontinuity between the nucleating agent and the surrounding polymer may lead to a local pressure field that is different from the bulk.

According to the classical nucleation theory [17-18], both the free energy barrier for heterogeneous nucleation (W_{het}) and the critical radius for bubble nucleation (R_{cr}) depend on the local pressure in the polymer matrix:

$$W_{het} = \frac{16\pi\gamma_{lg}^{3} F(\theta_c, \beta)}{3\left(P_{bub,cr} - P_{sys}\right)^2} \quad (1)$$

$$R_{cr} = \frac{2\gamma_{lg}}{P_{bub,cr} - P_{sys}} \quad (2)$$

where γ_{lg} is the surface tension at the polymer-gas interface; $P_{bub,cr}$ is the pressure in a critical bubble; and P_{sys} is the local pressure in the polymer matrix; F is the ratio of the volume of the heterogeneously nucleated bubble to the volume of a spherical bubble having the same radius; parameters θ_c and β are related to interfacial properties of a particle and the geometry of the particle respectively.

While pioneering studies [19-21] provide some qualitative insights into stress-induced cell nucleation, this paper is the first endeavor to study the local stress field around heterogeneous nucleating sites during polymeric foaming processes. As a result, it aims to provide new information about the underlying mechanism that promotes cell nucleation in the presence of heterogeneous nucleating agents. The results are from a numerical model that model pressure changes in response to given conditions. The presence of the nucleating agents makes the polymer melt mixture a two-phase material, and so an interface tracking method (ALE formulation and a mesh-updating technique) were developed to track the moving boundaries within the filed, while the flow itself was solved as a single phase.

In the following sections, a mathematical model based on the physical laws and assumptions is introduced; the numerical algorithm for solving the pressure field around a heterogeneous nucleating site is explained; and finally, several cases are studied and the simulation results are presented.

Methodology

Interface Tracking Method

The mixture of polymer melt and blowing agent can be considered to be a single-phase fluid. However, the presence of *0.5-5wt%* solid nano-clay or mineral oil makes the mixture a two-phase (liquid and solid, or liquid and liquid) material. In this study, an interface tracking method is used, and yet the different phases are treated as a single-phase, and so a single set of governing equations are solved for the whole computational domain. The interface tracking method has been widely used [22-24] in numerical modeling to treat a multiphase flow as a single phase. It is a suitable method for this study because the weight percent of the clay is small, and only a nano-scale site is considered. The modeling is carried out for the mixture of polymer melt, and the interface between the polymer melt and the solid clay is tracked explicitly by an unstructured adaptive mesh.

Conservation Laws

The mixture of polymer melt and blowing agent consisting of nucleating agent particles is assumed to be a single-phase mixture, and the flow is assumed incompressible and steady state, if the particle does not move; the flow is assumed to be unsteady if the particle moves with the flow field or deforms due to the shear stress of the flow. The flow complies with conservation laws for mass and momentum, which are in the form of a set of partial differential equations:

$$\nabla \cdot u = 0 \tag{3}$$

$$\rho \frac{DU}{Dt} = \nabla \bullet \sigma + f \tag{4}$$

u is the velocity vector, σ is the stress tensor, ρ is fluid density, and *f* is an external force term. The stress tensor is required to obey the constitutive equations:

$$\sigma = -PI + \tau \tag{5}$$

and

$$\tau = 2\mu(\dot{\gamma})d \tag{6}$$

where *P* is the fluid pressure, *I* is the identity tensor, μ is the dynamic viscosity, and *d* is the rate-of deformation tensor given by:

$$d = \frac{1}{2}\left[\left(\nabla u\right) + \left(\nabla u\right)^T\right] \tag{7}$$

where $\dot{\gamma}$ is the local shear rate defined by

$$\dot{\gamma} = \sqrt{2tr(d \cdot d)} \tag{8}$$

The polymer melt is modeled as a purely viscous fluid, where the shear rate $(\dot{\gamma})$ dependent viscosity of the melt is described by a power-law model:

$$\mu(\dot{\gamma}) = m(\dot{\gamma})^{n-1} \tag{9}$$

where *m* is the consistency index and n is the power-law index. In this case, an isothermal condition was assumed.

ALE Formulation

The arbitrary Lagrangian-Eulerian (ALE) formulation is applied to describe the interface between the polymer melt mixture and the solid clay or mineral oil. The ALE formulation is a generalized kinematic description that allows arbitrary mesh movement with the mesh velocity decoupled from the fluid velocity. The governing equations (3) and (4) are non-dimensionalized by introducing a non-dimensional Reynolds number $\mathrm{Re} = UL/\mu$. L is a flow characteristic length, U is a characteristic velocity and μ is the dynamic viscosity. The non-dimensional form of the governing equations (neglecting the external term) after the ALE formulation is applied, is:

$$\nabla \cdot u = 0 \tag{10}$$

$$\alpha^2 \frac{\partial u}{\partial t} + \mathrm{Re}(u - u^G)\nabla u = -\mathrm{Re}_1 \nabla P + \nabla \bullet [\mu \bullet (\nabla u) + (\nabla u)^T] \tag{11}$$

where u^G is the mesh velocity. If the nucleating clay does not deform or is not moving with the flow, $u^G = 0$; otherwise, a moving boundary case is considered. For molten polymer flow, the Reynolds number is very small, usually in the range of $10^{-4} - 10^{-2}$.

Numerical Algorithm

The governing equations (10) and (11) are spatially discretized using a Galerkin finite element approach in conjunction with P2-P1 tetrahedral Taylor-Hood elements. The unknown velocity and pressure fields are expressed in terms of the shape functions ϕ_j and ψ_j and the nodal velocity and pressure values u_j and p_j:

$$u = \sum_{j=1}^{N} u_j \varphi_j \tag{12}$$

$$p = \sum_{j=1}^{N_p} p_j \psi_j \tag{13}$$

where there are $N = 10$ degrees of freedom for velocity (in each co-ordinate direction) and temperature, and $N_p = 4$ degrees of freedom for pressure. Following a Galerkin spatial discretization, the governing equations are written in semi-discrete form as:

$$[M]\frac{d\{u\}}{dt} + ([N] - [N^G]) + [S]\{u\} + [L]^T\{p\} = \int_\Gamma (-pn + \frac{\partial u}{\partial n})\, dS \tag{14}$$

$$[L]\{u\} = 0 \tag{15}$$

where $\{u\}$ and $\{p\}$ are the vectors of nodal velocity and pressure. $[M]$, $[S]$ and $[L]$ are elemental matrices, *S* is the boundary of the elemental volume, and n is a normal vector.

Mesh Deformation

In modeling flow problems with moving boundaries, a technique needs to be applied to update the mesh when the domain deforms. A widely used approach is the spring analogy method, in which the edges of the mesh elements are considered to be fictitious springs. In this work, the semi-torsional spring analogy method is used to describe the movement of the mesh as the clay or mineral oil droplet moves. The semi-torsional spring analogy isderived from the lineal spring analogy and the torsional spring analogy by defining the stiffness of an edge (edge *i-j*) of an element as the sum of its lineal stiffness and its semi-torsional stiffness:

$$k_{ij} = k_{ij}^{\ lineal} + k_{ij}^{\ semi-torsional} \tag{16}$$

where $k_{ij}^{\ lineal}$ can be defined by the coordinates of the two nodes connected by an edge, and $k_{ij}^{\ semi-torsional}$ is defined as:

$$k_{ij}^{\ semi-torsional} = \sum_{m=1}^{NE_{ij}} \frac{1}{\sin^2 \theta_m^{\ ij}} \tag{17}$$

where NE_{ij} is the number of elements sharing edge *i-j,* and $\theta_m^{\ ij}$ is the facing angle, defined as the angle that faces the edge *i-j* on the *m*th element attached to the edge.

The mesh-updating algorithm is implemented in a FEM code [25] for solving the 3D incompressible NS equations in an ALE formulation. The implementation was validated using flows with moving boundaries for simple cases.

Results and Discussion

The numerical modeling is carried out for several cases. First, a solid rectangular plate, which can represent a particle or a group of particles of the nucleating agent (e.g., talc) in a polymer melt mixture, is considered. The plate may stick to a spot during foaming, when it is a group of particles; or move with the mixture flow, if it is a nano-scale particle. The movement can also be multiplex: it can simply move in the flow direction, spin due to shearing, or move randomly. Some results of these cases are presented, to illustrate how pressure changes around the plate, as a function of the dimension aspect ratio of the plate. Second, the pressure profile inside a nano-scale cavity on a solid wall (which could be a clay particle) was studied. The effects of the flow rate and of the cavity angle on the pressure profile were investigated. Finally, numerical simulations were carried out for cases involving a mineral ball, as it deforms or does not deform when the polymer melt mixture is stretched or squeezed. A summary of all the cases studied is listed in Table 1.

Geometry of the Nucleating Sites and Parameters

A 3D volume of a rectangular plate or of a sphere is considered to be the geometry for Cases I and III. The rectangular plate or the sphere represents a solid nucleating clay or mineral droplet submerged in the mixture of the polymer melt and blowing agent. Figure 1 shows part of the numerical volume. Figure 3 shows the spatial discretization, which is the finite element mesh for the geometry of case III.

The material considered in this study is WB130HMS polypropylene (PP) with 2 wt% CO_2. An isothermal condition was assumed. Both flow rate representative of extrusion conditions and of batch foaming conditions were studied. A summary of material data used for the calculations, and the operating conditions considered, are listed in Table 2.

Case I: Solid Plate in a Polymer Melt Mixture

Consider a solid plate (or a plate formed by conglomerated particles) that is immovable in an upward flowing polymer melt mixture. The simulation result of the pressure profile is shown in Figure 4, and indicates that a) the pressure around the solid plate is significantly different from that of the mixture; b) in the flow direction, there are extreme values of pressure at the top and the bottom of the plate; c) the pressure values at the top of the plate are negative. The negative pressure values around a solid particle are beneficial to cell nucleation because they will promote supersaturation; and this result can then be used to explain the cell propagation in this area as the flow field caused by the growth of the nucleated bubbles [26]. The pressure was plotted along the line AA in Figure 4, and the effect of the dimensional aspect ratio on the pressure profile is shown in Figure 5. As the aspect ratio *a:b* (equals to 4:1 (a flat plate), 1:1 (a cube), and 1:4 (a thin slat)) varies, the pressure at the top and the bottom of the plate decreases although the pressure distribution for each case is the same.

Second, consider a plate (a clay particle) that is moving with the flow field. The pressure changes with time along the line that goes through the top and the bottom of the plate, is shown in Figure 6. The pressure distribution is different from Figure 4, in which case the particle is immovable. Also, the pressure on the surface (top or bottom) is smaller than when it does not move; and the pressure change is not abrupt as in Figure 6. In addition, the negative pressure area is bigger than the previous case for the fixed clay particle, which makes the pressure profiles on the top and the bottom nearly symmetric. This is because, although the plate is moving with the flow field, there is no relative movement between the plate and the mixture, and therefore, the pressure around the plate is close to the pressure of the mixture.

Third, consider a solid plate spinning in a shear flow, either spinning about a fixed corner, or spinning and moving forward at the same time. A schematic is shown in Figure 7. The pressure profile along the line BB (Figure 8) was plotted against time. At the beginning, when the plate starts to spin, the pressure around the particle is high, but then the pressure approaches a

constant value that the pressure is still higher than that of the mixture. Moreover, the pressure profile is higher than the case when the plate is immovable (Figure 5). This may due to the effect of shear on the plate. Figure 9 illustrates the pressure profile along BB in Figure 7, but for the plate that is spinning and moving forward at the same time. Although similar pressure profiles are involved, the latter case results in a smaller pressure variations around the plate.

Case II: Cavity on a Clay Surface

Consider a nano-scale cavity (small but still large enough to have a flow field inside) along a solid wall, with the polymer melt flow above the cavity, Figure 2. The pressure field in and around the cavity is shown in Figure 10, which shows the polymer melt mixture flowing above the cavity generates a sharp pressure change at the edge of the cavity. This is because the flow field encounters a significant change near the cavity, which makes it a potential nucleation site. The pressure change along line AA in Figure 10 was plotted; the effect of the flow rate on the pressure profile is shown in Figure 11. Two flow rates were considered for the polymer melt mixture above the cavity: one is relatively high, as for an extrusion condition; the other is very low, as for the batch foaming condition. Figure 11 indicates that as the flow rate increases, the pressure around the edge of the cavity also increases. The pressure profiles for both the high and low flow rate cases are similar because the same cavity is involved. The effect of the cavity angle on the pressure field was also investigated. The pressure profile along AA for different cavity angles θ (sharp to wide, $\theta = 30^o, 60^o, 90^o$) is plotted in Figure 12. It clearly shows that as the cavity angle becomes sharp, the pressure also changes dramatically, which indicates that a sharper cavity will be advantageous to cell nucleation.

Case III: Deforming Sphere in a Polymer Mixture

A sphere or a droplet in a mixture of polymer melt is the third case considered. The sphere is assumed either to be solid clay or a mineral oil droplet that can be deformed. The simulation was carried out for the case of a solid sphere when the polymer mixture is stretched. The pressure profile is shown in Figure 13. In this case, all the values of the pressure profile around the sphere are negative, and the pressure profiles at the left and the right hand sides of the sphere are larger than at the top and bottom. Similarly, this large area with negative pressure is a place where more cell propagation can be induced. Figure 14 shows the pressure profile changes along line AA in Figure 13 as time changes. Finally the surface stress on a squeezed sphere can be calculated. When the spherical droplet is deformed, the stress changes at the surface of the droplet with a symmetric stress distribution at the top and the bottom of the sphere.

Conclusions

Pressure is an important parameter that affects cell nucleation. The presence of cell nucleating agents that promote cell nucleation creates discontinuities in the foaming mixture. Knowledge of the pressure variation and distribution around a nucleation site is a key to understanding the underlying mechanism that promotes cell nucleation. To highlight this, numerical simulations of the pressure profiles around nucleating sites in a mixture of polymer melt and blowing agent have been calculated. Several cases were studied and, the issues that affect pressure distribution were investigated. The pressure profile around nucleating agents can vary significantly from the surrounding. Area where involves negative pressure distribution can induce cell propagation and the cell nucleation rate can be high. A cavity in a processing wall has an effect on pressure profile, and different geometry of a cavity results in different pressure distribution. Nucleating site that is involved in stretching will significantly promote heterogeneous nucleation. Finally, a deformed particle in a mixture induces a change of the nearby stress and pressure fields, which is also beneficial to cell nucleation.

Acknowledgments

The authors are grateful to the Ontario Centres of Excellence (OCE) and the Consortium for Cellular and Microcellular Plastics (CCMCP) at the University of Toronto for the financial support of this study.

References

1. D.F. Baldwin and N.P. Suh, *SPE-ANTEC Tech Papers*, 38, 1503 (1992).
2. K.A. Seeler and V. Kumar, *ASME, Cellu. Polym.*, 38, 93 (1992).
3. L. Glicksman, *Notes from MIT Sum Prog 4.10S Foam and Cellu. Mater: Therm. and Mech. Prop.*, Cambridge, MA, June 29-1 (1992).
4. K.W. Suh, C.P. Park, M.J. Maurer, M.H. Tusim, R.D. Genova, R. Broos, and D.P. Sophiea, *Adv Mater*, 12, 1779 (2000).
5. A. Kabumoto, N. Yoshida, M. Itoh, and M. Okada, US Patent 5844731 (1998).
6. J.H. Han, and C.D. Han, *J. Polym. Sci.*, 28, 743 (1990).
7. D. Turnbull, and B. Vonnegut, *Ind. Eng. Chem.*, 44, 1292 (1952).
8. N.H. Fletcher, *J. Chem. Phys.*, 29, 572 (1958).
9. N.H. Fletcher, *J. Chem. Phys.*, 31, 1136 (1959).
10. R. Cole, *Adv. Heat Trans.*, 10, 85 (1974).

11. J.G. Lee, and R.W. Flumerfelt, *J. Coll. Int. Sci.*, 184, 335 (1996).
12. M.A. Shafi, K. Joshi, and R.W. Flumerfelt, *Chem. Eng. Sci.*, 52, 635 (1997).
13. K. Joshi, J.G. Lee, M. Shafi, and R.W. Flumerfelt, *J. App. Polym. Sci.*, 67, 1353 (1998).
14. M. Shimoda, I. Tsujimura, M. Tanigaki, and M. Ohshima, *J. Cellu. Plast.*, 3**7**, 517 (2001).
15. D. Mao, J.R. Edwards, and A. Harvey, *Chem. Eng. Sci.*, 61, 1836 (2006).
16. S.N. Leung, C.B. Park, and H. Li, *Plastics, Rubber and Composites: Macromolecular Engineering*, 35, 93 (2006).
17. Gibbs, J.W., *The Scientific Papers of J. Willard Gibbs, Vol. 1*; Dover: New York, 337 (1961)..
18. Blander, M., and Katz, J. L., *AIChE J*, 21, 833 (1975).
19. S.T. Lee, *Polym. Eng. Sci.*, 33, 418 (1993).
20. L. Chen, H. Sheth, and X. Wang, *J. Celul. Plast.*, 37, 353 (2001).
21. C.Y. Gao, N.Q. Zhou, X.F. Peng, and P. Zhang, *Polym. Plast. Tech. Eng.*, 45, 1025 (2006).
22. M. Sussman, E. Fatemi, An efficient interface preserving level set redistancing algorithm and its application to interfacial incompressible fluid flow, *SIAM J. Sci Comp,* vol. 20, pp. 1165-1191 (1999).
23. D. Lakehal, M. Meier and M. Fulgosi, Interface tracking towards the direct simulation of heat and mass transfer in multiphase flows, *Int. J. of Heat and Fluid Flow*, 23, pp. 242–257 (2002).
24. U. Salih O, T. Gretar, A front-tracking method for viscous, incompressible, multi-fluid flows, *J. Comp Phys*, vol. 100, no. 1, p. 25-37 (1992).
25. P. Minev and C. Ethier, A characteristic/finite element algorithm for time dependent 3-D advection-dominated transport using unstructured grids, *Comp Meth* Appl Mech *Eng* 192:1281–1298 (2003).
26. S. N. Leung, A. Wong, and C. B. Park, A new interpretation to the talc-enhanced polymeric foaming, *SPE ANTEC Tech Papers* (2009).

Table 1. Numerical simulation cases

Cases	**Case I**	**Case II**	**Case III**
Geometry	Rectangular plate in a volume	Cavity on a solid (clay) wall	Ball in a volume
Flow Rate	High	High/Low	Low
Cavity Angle	-	30, 60, 90	-
Aspect Ratio	Rectangle / Cube / Thin	-	-
Boundary Movement	Fixed / Spin / Random	Fixed	Fixed / Straight motion
Deformation	No	No	squeezing

Table 2. Material data and operating conditions

Parameters	**Values**
Density (*g/ml*)	0.910
CO_2 Content (*wt%*)	2.0
Power-Law Index (*n*)	0.4
Power-Law Consistency ($pa \bullet s^n$)	5100
Reynolds Number (*Re*)	1.0×10^{-4}
Flow-Rate (*g/s*)	20 /0.002
Melt Temperature (*T*)	190

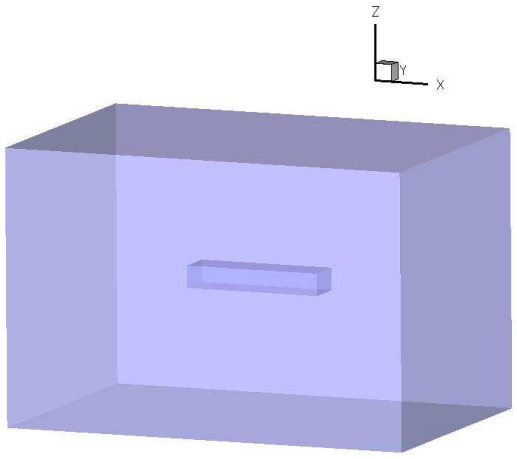

Figure 1. Numerical geometry for Case I

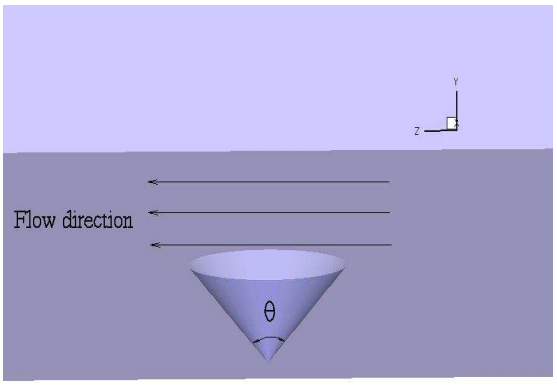

Figure 2. Numerical geometry for case II

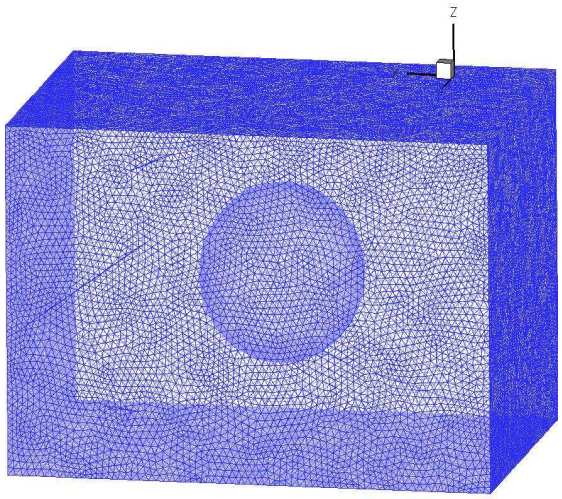

Figure 3. 3D Mesh for the geometry of case III

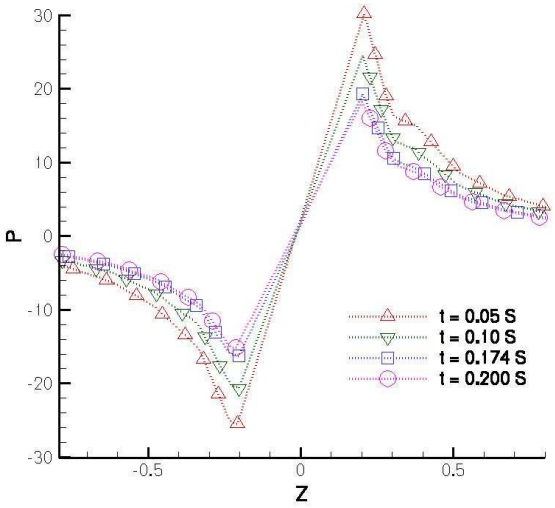

Figure 6. Pressure along line AA in Figure 4 as time changes

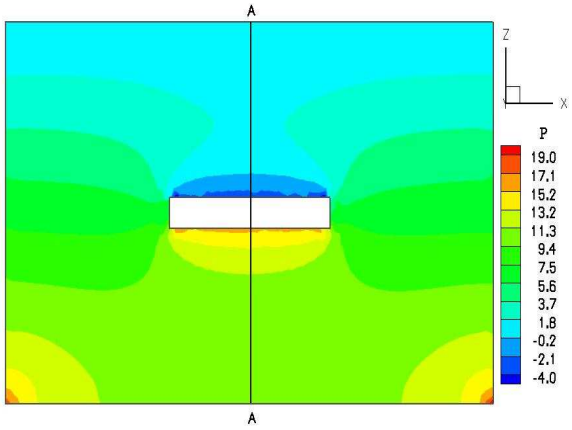

Figure 4. Pressure contour for Case I

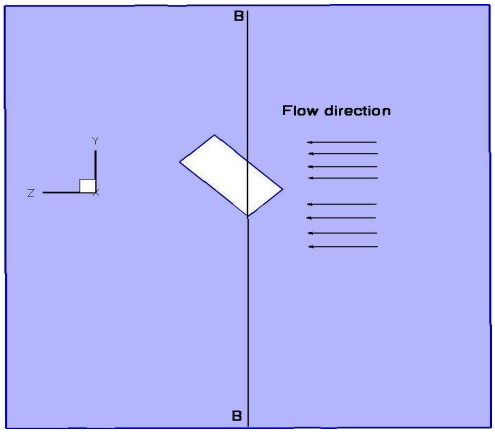

Figure 7. Solid plate in shear flow

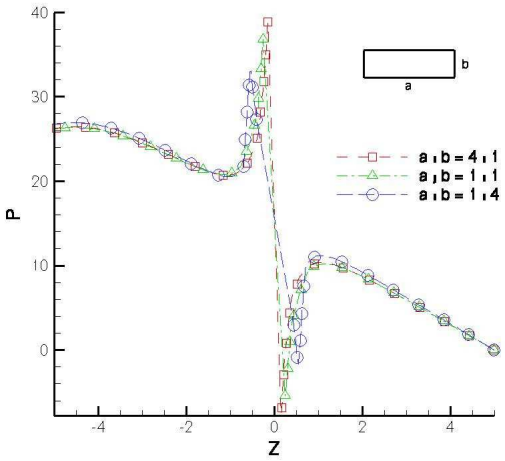

Figure 5. Pressure profile along line AA in Figure 4; effect of the aspect ratio on pressure distribution

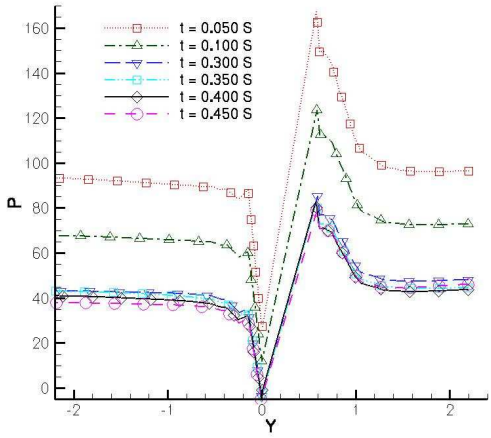

Figure 8. Pressure at line BB when the plate is spinning

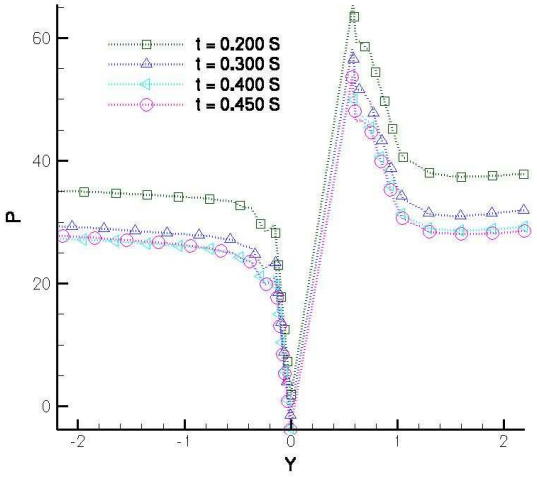

Figure 9. Pressure along line BB (Figure 7) when the plate is spinning and moving forward at the same time

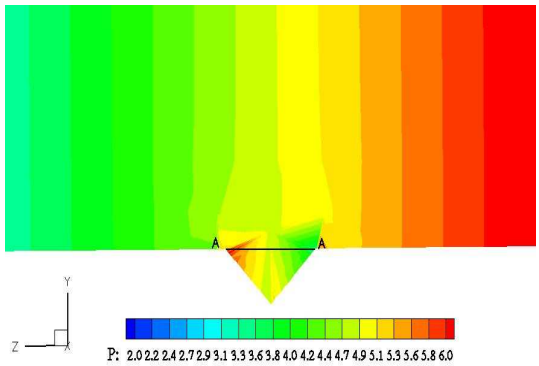

Figure 10. Pressure profile around a cavity

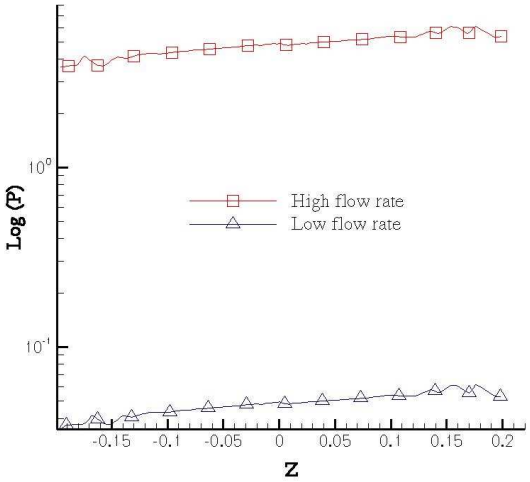

Figure 11. Pressure along line A-A in Figure 10

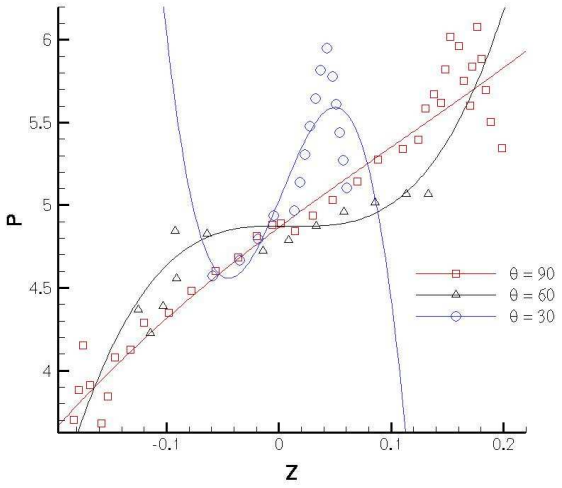

Figure 12. The effect of cavity angle on pressure

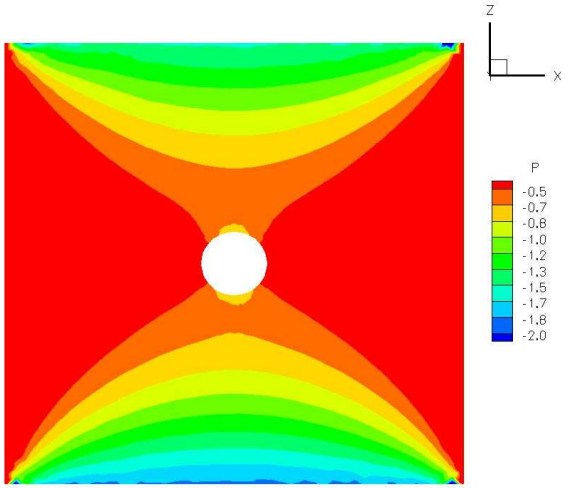

Figure 13. Pressure profile when the mixture is stretched

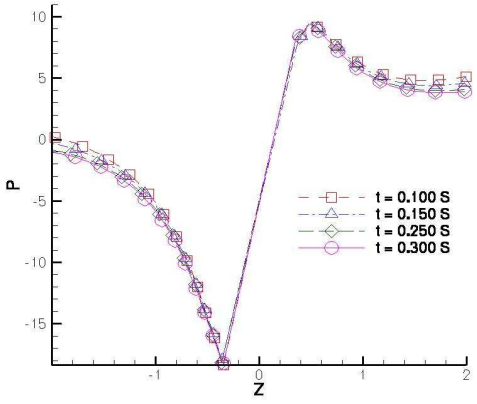

Figure 14. Pressure profile along line through the top and bottom of the squeezed sphere